

Soft band X/K luminosity ratios in late-type galaxies and constraints on the population of supersoft X-ray sources

Á. Bogdán¹* and M. Gilfanov^{1,2}*

¹Max-Planck-Institut für Astrophysik, Karl-Schwarzschild-Str.1, 85741 Garching bei München, Germany

²Space Research Institute, Russian Academy of Sciences, Profsoyuznaya 84/32, 117997 Moscow, Russia

ABSTRACT

We study X-ray to K-band luminosity ratios (L_X/L_K) of late-type galaxies in the 0.3 – 0.7 keV energy range. From the *Chandra* archive, we selected nine spiral and three irregular galaxies with point source detection sensitivity better than $5 \cdot 10^{36} \text{ erg s}^{-1}$ in order to minimize the contribution of unresolved X-ray binaries. In late-type galaxies cold gas and dust may cause significant interstellar absorption, therefore we also demanded the existence of publicly available HI maps. The obtained L_X/L_K ratios vary between $(5.4 - 68) \cdot 10^{27} \text{ erg s}^{-1} L_{K,\odot}^{-1}$ exceeding by factor of 2 – 20 the values obtained for gas-poor early-type galaxies. Based on these results we constrain the role of supersoft X-ray sources as progenitors of type Ia supernovae (SNe Ia). For majority of galaxies the upper limits range from $\sim 3\%$ to $\sim 15\%$ of the SN Ia frequency inferred from K-band luminosity, but for a few of them no meaningful constraints can be placed. On a more detailed level, we study individual structural components of spiral galaxies: bulge and disk, and, for grand design spiral galaxies, arm and interarm regions.

Key words: Galaxies: irregular – Galaxies: spiral – Galaxies: stellar content – Supernovae: general – X-rays: galaxies – X-rays: stars

1 INTRODUCTION

SNe Ia are “standardizable candles” and hence can be used to determine the cosmological distance scale. Thus, they played a major role in establishing that the Universe is expanding at an accelerating rate, which fact directly pointed at the existence of the dark energy (Riess et al. 1998; Perlmutter et al. 1999). Despite the vast importance of SNe Ia, their progenitor systems are still debated.

Recently we proposed an argument significantly constraining progenitor scenarios of SNe Ia in early-type galaxies (Gilfanov & Bogdán 2010). We pointed out that the combined energy output of accreting and steady nuclear burning white dwarfs can be used to measure the rate at which white dwarfs increase their mass in galaxies. Thus, the contribution of the single degenerate scenario to the observed SN Ia frequency could be constrained. We concluded that in early-type galaxies no more than $\sim 5\%$ of SNe Ia are produced by white dwarfs accreting from a donor star in a binary system and detonating at the Chandrasekhar mass. Along similar (but not identical) line of arguments Di Stefano (2010) compared numbers of supersoft sources detected in several nearby elliptical and spiral galaxies with predictions of the single-degenerate scenario and found a discrepancy of about 2 orders of magnitude.

It is tempting to apply the arguments of Gilfanov & Bogdán

(2010) to spiral and irregular galaxies. However, it is important to realize that in case of late-type galaxies constraints on the X-ray output of accreting white dwarfs do not necessary lead to equally constraining upper limits on the contribution of the single-degenerate scenario. In young stellar environment several channels exist in which X-ray emission from growing white dwarfs may be significantly suppressed. These include high accretion rate configurations with optically-thick wind having large photospheric radius (Hachisu et al. 1996, 1999), and white dwarfs accreting He-rich material, characterized by about an order of magnitude smaller nuclear energy release (Iben & Tutukov 1994). (Note that these channels are not expected to play significant role in much older elliptical galaxies considered by Gilfanov & Bogdán (2010).) Nevertheless, measurements of L_X/L_K ratios are of much interest for late-type galaxies as well as they do constrain the populations of supersoft X-ray sources and their possible role as progenitors of SNe Ia. This question is in the focus of the present paper.

There are several other important differences between late- and early-type galaxies relevant to this study. Firstly, it is the amount of cold interstellar gas and dust, absorbing the soft X-ray radiation from nuclear burning white dwarfs. Whereas it is negligible in elliptical galaxies, the enhanced and spatially variable absorption in younger galaxies strongly influences the observable X-ray emission from supersoft sources. This needs to be taken into account in comparing observations with predictions of SN Ia progenitor models. Secondly, it is the presence and magnitude of other X-ray emitting components in late-type galaxies, of which most im-

* E-mail: bogdan@mpa-garching.mpg.de (ÁB); gilfanov@mpa-garching.mpg.de (MG)

Table 1. The list of late-type galaxies studied in this paper.

Name	Distance (Mpc)	L_K ($L_{K,\odot}$)	N_H (cm^{-2})	Morphological type	SFR ($M_\odot \text{ yr}^{-1}$)	T_{obs} (ks)	T_{filt} (ks)	L_{lim} (erg s^{-1})	R (")
	(1)	(2)	(3)	(4)	(5)	(6)	(7)	(8)	(9)
M51	8.0 ^a	$6.4 \cdot 10^{10}$	$1.6 \cdot 10^{20}$	SABc	3.9	90.9	80.8	$3 \cdot 10^{36}$	175
M74	7.3 ^a	$1.6 \cdot 10^{10}$	$4.8 \cdot 10^{20}$	SA(s)c	1.1	104.4	84.7	$2 \cdot 10^{36}$	140
M81	3.6 ^b	$5.4 \cdot 10^{10}$	$4.1 \cdot 10^{20}$	SA(s)ab	0.4	239.1	202.1	$3 \cdot 10^{35}$	250
M83	4.5 ^a	$3.9 \cdot 10^{10}$	$3.9 \cdot 10^{20}$	SAB(s)c	2.8	61.6	52.1	$1 \cdot 10^{36}$	200
M94	4.7 ^a	$3.3 \cdot 10^{10}$	$1.4 \cdot 10^{20}$	(R)SA(r)ab	1.2	76.9	69.5	$1 \cdot 10^{36}$	164
M95	10.1 ^a	$3.3 \cdot 10^{10}$	$2.9 \cdot 10^{20}$	SB(r)b	1.1	120.1	99.6	$3 \cdot 10^{36}$	88
M101	7.4 ^a	$3.4 \cdot 10^{10}$	$1.2 \cdot 10^{20}$	SAB(rs)cd	1.3	1070.6	833.3	$2 \cdot 10^{35}$	167
NGC2403	3.2 ^b	$5.0 \cdot 10^9$	$4.2 \cdot 10^{20}$	SAB(s)cd	0.4	224.0	184.2	$2 \cdot 10^{35}$	140
NGC3077	3.8 ^a	$2.6 \cdot 10^9$	$4.0 \cdot 10^{20}$	I0 pec	0.3	54.1	42.1	$1 \cdot 10^{36}$	77.5
NGC3184	11.1 ^c	$2.7 \cdot 10^{10}$	$1.1 \cdot 10^{20}$	SAB(rs)cd	1.1	66.7	45.2	$5 \cdot 10^{36}$	140
NGC4214	2.9 ^a	$6.5 \cdot 10^8$	$1.5 \cdot 10^{20}$	IAB(s)m	0.2	83.4	53.6	$4 \cdot 10^{35}$	70
NGC4449	4.2 ^a	$3.4 \cdot 10^9$	$1.4 \cdot 10^{20}$	IBm	0.4	102.1	97.0	$6 \cdot 10^{35}$	95

Note. Columns are as follows. (1) Distances. References are: ^a Karachentsev et al. (2004) – ^b Freedman et al. (2001) – ^c Leonard et al. (2004). (2) Total near-infrared luminosity of the elliptic region described in column (9). (3) Galactic absorption (Dickey & Lockman 1990). (4) Taken from NED (<http://nedwww.ipac.caltech.edu/>). (5) Star-formation rate within the same ellipse. (6) and (7) Exposure times before and after data filtering. (8) Point source detection sensitivity in the 0.5 – 8 keV energy range. (9) Major axis of the studied elliptic regions. The orientation and shape of the regions were taken from K-band measurements (<http://irsa.ipac.caltech.edu/applications/2MASS/>).

portant is ionized hot ISM. Whereas it is possible to find gas-free galaxies among ellipticals, all late-type galaxies appear to contain moderate to large amount of X-ray emitting gas. The exact distribution of this gas cannot be determined a priori, hence its contribution cannot be separated and removed from other X-ray emitting components. In late-type galaxies high-mass X-ray binaries (HMXBs), located in star-forming regions, also can make a notable contribution (Grimm et al. 2003), and similarly to ellipticals, the population of low-mass X-ray binaries (LMXBs) is also present with luminosities down to $\sim 10^{35} \text{ erg s}^{-1}$ (Gilfanov 2004). Other type of faint unresolved sources, such as coronally active binaries, proto-stars, and young stars (Sazonov et al. 2006) also contribute to the observed soft X-ray emission. As all these components cannot be differentiated, we can only give upper limits on the X-ray emission from the population of supersoft sources. Although same is true for early-type galaxies, the magnitude of contaminating factors is significantly larger in late-type galaxies.

The paper is structured as follows: in Sect. 2 we describe the sample selection and in Sect. 3 we introduce the analyzed data and discuss its reduction. The various X-ray emitting components are overviewed in Sect. 4 and the observed L_X/L_K ratios are presented in Sect. 5. In Sect. 6 we investigate the role of supersoft sources as SN Ia progenitors. We summarize in Sect. 7.

2 SAMPLE SELECTION

We aim to select a broad sample of nearby late-type galaxies, including spirals and irregulars. Precise knowledge of intrinsic absorption is critical for the comparison of observed X-ray luminosities with predictions of SN Ia models. Therefore face-on galaxies are preferred due to the lack of projection effects. In a recent study Walter et al. (2008) studied the HI distribution of 34 nearby galaxies in full particulars. We used this sample as a starting point, as

substantial fraction of their selected galaxies is well observed in X-ray wavelengths. The sample was filtered by demanding deep *Chandra* observations, allowing to achieve a point source detection sensitivity of $\lesssim 5 \cdot 10^{36} \text{ erg s}^{-1}$ in the 0.5 – 8 keV energy band. With this sensitivity we expect that the contribution of unresolved LMXBs and HMXBs do not influence significantly the observed L_X/L_K ratios – for quantitative analysis see Sect. 4.3. There are 16 galaxies fulfilling these criteria. However, in case of four low-mass irregular galaxies (DDO53, DDO154, Holmberg I, IC2574) the total number of observed X-ray counts is too low to perform a detailed analysis, hence we excluded them from our sample.

The final list of galaxies consists of nine spiral and three irregular galaxies, whose main properties are listed in Table 1.

3 DATA REDUCTION

3.1 *Chandra* data

We analyzed all publicly available observations of the selected galaxies which had an exposure time longer than 2 ks. Totally, this yielded 71 observations (status: 06/2010). The overall exposure time of the data was $T_{\text{obs}} \approx 2.3 \text{ Msec}$. For each observation we extracted data of the S3 chip, except for Obs-ID 9553, where we used the entire ACIS-I array. The data was reduced with standard CIAO¹ software package tools (CIAO version 4.1; CALDB version 4.1.3).

The data reduction was performed similarly to that described in Bogdán & Gilfanov (2008). First, we filtered the flare contaminated time intervals, after which the exposure time decreased by

¹ <http://xc.harvard.edu/ciao>

$\lesssim 20\%$. The observed and filtered exposure times of the combined data are listed in Table 1. However, for point source detection the unfiltered data was used, since the longer exposure time outweighs the higher background periods. Observations for each galaxy were combined, they were projected in the coordinate system of the observation with the longest exposure time. To detect point sources we ran the CIAO wvdetect tool on the merged data separately in the 0.3 – 0.7 keV and in the 0.5 – 8 keV energy range, resulting source lists were combined. For the source detection algorithm we applied the same parameters that were discussed in Bogdán & Gilfanov (2008). Accordingly, the obtained elliptic source regions contain large fraction, $\gtrsim 98\%$, of source counts. These output source cells were used to mask out point sources for further analysis of the unresolved emission. Note, that the source detection sensitivities (L_{lim}), given in Table 1, refer to the 0.5 – 8 keV band and are computed assuming 10 net counts.

For galaxies significantly smaller than the field of view we estimated the background components using a combination of a number of regions away from galaxies. The angular size of four galaxies (M51, M74, M81, M83) exceeds or is comparable with the extent of the combined Chandra image, therefore we used the ACIS “blank-sky” files² to estimate the background. As the instrumental background components of *Chandra* vary with time, we renormalized the background counts using the 10 – 12 keV count rates. To obtain point source detection sensitivities in the 0.5 – 8 keV energy range, we produced exposure maps assuming a power-law model with a slope of $\Gamma = 2$. In the 0.3 – 0.7 keV band we used exposure maps computed by assuming $N_H = 10^{21} \text{ cm}^{-2}$ and a blackbody spectrum with $kT = 100 \text{ eV}$.

3.2 Infrared and HI data

The SN Ia rate in late-type galaxies can be either related directly to the mass of the galaxy (Mannucci et al. 2005) with the scale depending on the galaxy type, or it can be decomposed into a mass related and a star-formation related components (Sullivan et al. 2006). Thus, we need to trace both the stellar mass and the star formation rate (SFR). The near-infrared data of the 2MASS Large Galaxy Atlas (Jarrett et al. 2003) is known to be a good stellar mass tracer, hence we used K-band images for this purpose. The obtained 2MASS K-band images were background subtracted for all galaxies except for M51 and NGC3077, for these we estimated the background level by using several nearby regions off the galaxy.

The SFR was measured based on far-infrared images of the *Spitzer Space Telescope*. After obtaining the luminosity at $70 \mu\text{m}$ we converted it to total infrared luminosity (Bavouzet et al. 2008). This conversion incorporates notable systematic uncertainties whose measure depend on the employed far-infrared wavelength – the least, 19%, uncertainty applies for the $70 \mu\text{m}$ data. Detailed discussion about the sources of uncertainties can be found in Bavouzet et al. (2008). Based on the total infrared luminosities we computed the corresponding star-formation rates using Bell (2003). The scatter associated with the obtained star-formation rate depends on the total infrared luminosity of the galaxy: for $10^9 L_\odot$ and $10^{11} L_\odot$ it is 50% and 20%, respectively (Bell 2003). We note that no background is subtracted from the *Spitzer* $70 \mu\text{m}$ images, provided by the *Spitzer* archive, therefore we estimated it using nearby regions to the galaxies.

Late-type galaxies contain a large amount of cold gas and dust, associated with the active star formation, causing notable interstellar absorption. As our goal is to study a rather soft X-ray band, it is crucial to map its distribution and measure the absorbing column accurately. For this purpose we used the HI maps of Walter et al. (2008) which give detailed images of the neutral hydrogen content of galaxies.

4 SUPERSOFT SOURCES AND OTHER X-RAY EMITTING COMPONENTS IN LATE-TYPE GALAXIES

The goal of this investigation is to constrain the X-ray luminosity of nuclear burning white dwarfs. In order to maintain stable hydrogen burning on the surface of white dwarfs a rather high, $\dot{M} \gtrsim 10^{-7} M_\odot/\text{yr}$, accretion rate is required (Nomoto et al. 2007). The energy of hydrogen fusion is released in the form of electromagnetic radiation, with bolometric luminosity of $L_{\text{bol}} \sim 10^{37} - 10^{38} \text{ erg s}^{-1}$. The high bolometric luminosity means that some fraction of these sources may be detected by *Chandra* as supersoft X-ray sources. However, because of their low color temperature and large absorption in late-type galaxies, most of them will remain undetected by *Chandra* and will contribute to the unresolved soft emission. Obviously, in estimating the total X-ray output of nuclear burning white dwarfs, both resolved and unresolved supersoft sources need to be taken into account. However, there is a number of other X-ray emitting components contributing to unresolved emission in late-type galaxies, including genuinely diffuse emission from ionized ISM and various types of faint compact X-ray sources. These components play the role of contaminating factors in measuring the X-ray luminosity of nuclear burning white dwarfs, and, as discussed below, account for the significant fraction of unresolved soft X-ray emission in late-type galaxies. As emission from these components cannot be separated from each other, it is only possible to obtain upper limits on the X-ray luminosity of nuclear burning white dwarfs. Their real luminosity is likely to be smaller by a large (but unknown) factor.

4.1 Resolved supersoft sources

Bright supersoft sources were differentiated from other resolved point sources based on spectral properties. As the temperature of the hydrogen burning layer is in the range of $\sim 30 - 100 \text{ eV}$, we conservatively included all resolved sources with hardness ratios corresponding to the blackbody temperature of $kT_{\text{bb}} < 175 \text{ eV}$. Hardness ratios were computed based on three energy bands, 0.1 – 1.1 keV as soft, 1.1 – 2 keV as medium, and 2 – 7 keV as hard band, furthermore we applied the relations described by Di Stefano & Kong (2003) to identify supersoft sources. Their total observed luminosities are listed in Table 2.

4.2 Hot ionized gas

In late-type galaxies bright X-ray emission from hot ionized gas is expected. The total X-ray luminosity of this component may exceed the emission arising from unresolved compact X-ray sources. To reveal the presence of hot X-ray emitting gas we extracted spectra of the unresolved emission in the studied galaxies, shown in Fig. 1. For spirals we plot in the same panel the spectra of the bulge and the disk whereas for irregular galaxies the spectra

² <http://cxc.harvard.edu/contrib/maxim/acisbg/>

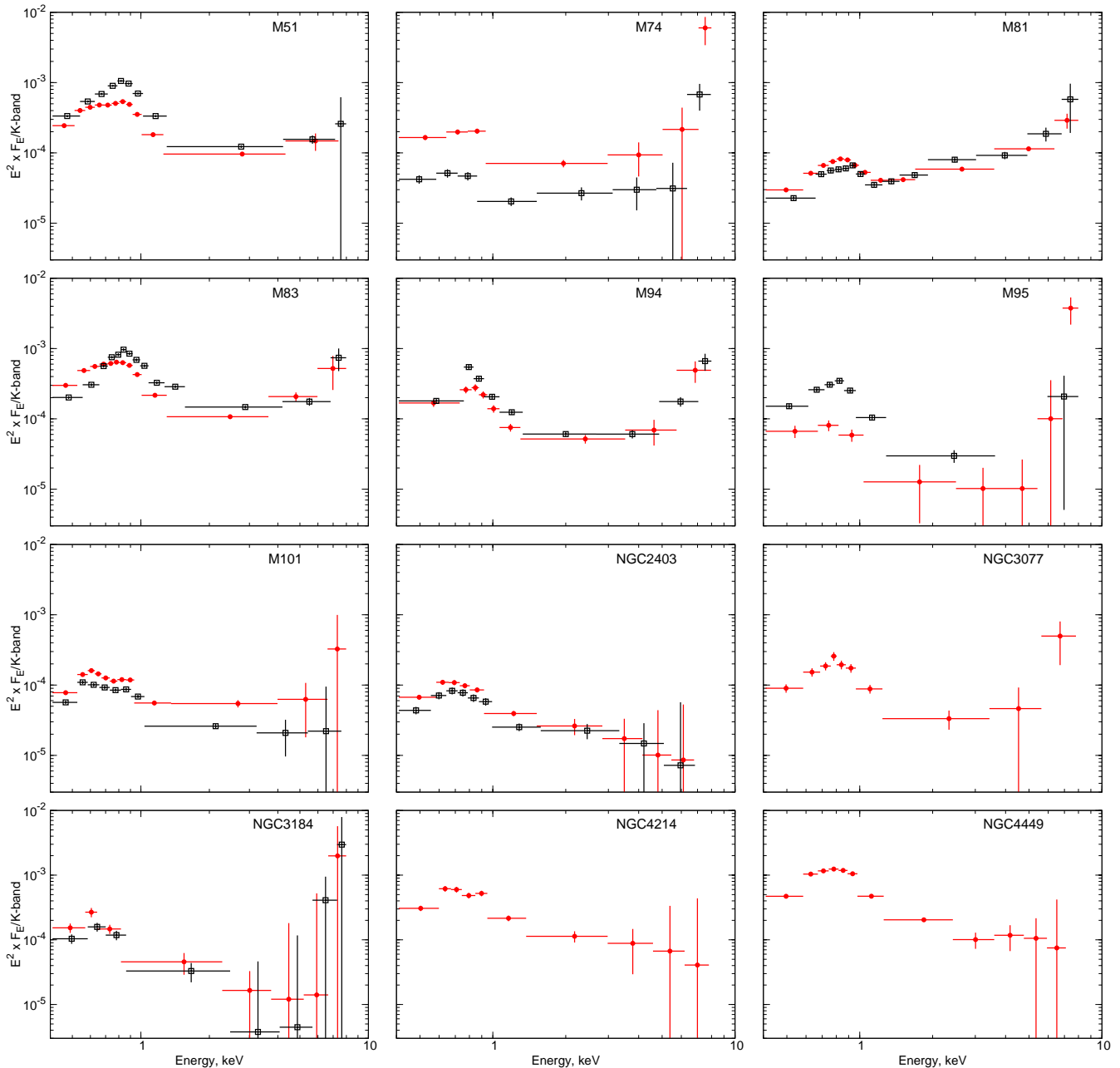


Figure 1. Energy spectra of the galaxies in our sample. To facilitate comparison all spectra were normalized to the same level of K-band brightness and rescaled to the same distance of 10 Mpc. All background components are subtracted. The scales on x- and y-axes are the same in all panels. For spiral galaxies, hollow squares (black) show the spectrum of the bulge, whereas filled circles (red) represent the spectrum of the disk.

refer to the entire galaxy. To facilitate the comparison we normalized them to the K-band luminosity of $10^{11} L_{K,\odot}$ and rescaled them to a distance of 10 Mpc.

In each galaxy we detect a strong soft component which is presumably due to hot X-ray emitting gas, completely dominating X-ray emission below ~ 1.5 keV. We performed spectral fits for each spectra and found that a two component model, consisting of an optically-thin thermal plasma emission model (MEKAL in XSPEC) and a power-law, gives an acceptable fit. As the main purpose of the present paper is to study the emission of unresolved supersoft sources, we do not study the results of spectral fits in details. Nevertheless, we mention that the best fit temperatures of the soft component are rather low, the obtained values are in the range

of $kT = 0.18 - 0.37$ keV. These values are too high to be attributed to the population of supersoft sources, where the temperature of the hydrogen burning layer is $\sim 30 - 100$ eV, hence this component originates most probably from hot ISM.

It is obvious from Fig. 1 that emission from the hot ISM dominates luminosity in the $0.3 - 0.7$ keV band. It is also obvious that it cannot be separated from other sources of soft X-ray emission. Therefore this is the main source of contamination in determining the luminosity of unresolved supersoft sources, much more significant than in the case of elliptical galaxies (Bogdán & Gilfanov 2010).

Table 2. X-ray luminosities in the 0.3 – 0.7 keV energy range of various X-ray emitting components in late-type galaxies.

Name	$N_{H,int}$ (cm^{-2})	$L_{X,unres}$ (erg s^{-1})	$L_{X,SSS}$ (erg s^{-1})	$(L_X/L_K)_{total}$ ($\text{erg s}^{-1} L_{K,\odot}^{-1}$)	$(L_X/L_K)_{bulge}$ ($\text{erg s}^{-1} L_{K,\odot}^{-1}$)	$(L_X/L_K)_{disk}$	$(L_X/L_K)_{arm}$	$(L_X/L_K)_{interarm}$	$(L_X/L_K)_{pred}$
	(1)	(2)	(3)	(4)	(5)	(6)	(7)	(8)	(9)
M51	$7.7 \cdot 10^{20}$	$2.7 \cdot 10^{39}$	$3.2 \cdot 10^{38}$	$4.7 \cdot 10^{28}$	$4.7 \cdot 10^{28}$	$4.5 \cdot 10^{28}$	$3.9 \cdot 10^{28}$	$5.0 \cdot 10^{28}$	$3.1 \cdot 10^{29}$
M74	$3.9 \cdot 10^{20}$	$2.6 \cdot 10^{38}$	$1.7 \cdot 10^{37}$	$1.7 \cdot 10^{28}$	$5.8 \cdot 10^{27}$	$2.3 \cdot 10^{28}$	$2.7 \cdot 10^{28}$	$2.1 \cdot 10^{28}$	$1.9 \cdot 10^{29}$
M81	$7.8 \cdot 10^{20}$	$1.4 \cdot 10^{38}$	$1.5 \cdot 10^{38}$	$5.4 \cdot 10^{27}$	$6.4 \cdot 10^{27}$	$3.4 \cdot 10^{27}$	$3.2 \cdot 10^{27}$	$3.6 \cdot 10^{27}$	$1.7 \cdot 10^{29}$
M83	$6.0 \cdot 10^{20}$	$1.6 \cdot 10^{39}$	$7.3 \cdot 10^{37}$	$4.3 \cdot 10^{28}$	$2.8 \cdot 10^{28}$	$5.2 \cdot 10^{28}$	$4.9 \cdot 10^{28}$	$5.5 \cdot 10^{28}$	$3.1 \cdot 10^{29}$
M94	$4.6 \cdot 10^{20}$	$2.9 \cdot 10^{38}$	$2.3 \cdot 10^{37}$	$9.5 \cdot 10^{27}$	$1.1 \cdot 10^{28}$	$7.0 \cdot 10^{27}$	–	–	$2.5 \cdot 10^{29}$
M95	$2.1 \cdot 10^{20}$	$3.9 \cdot 10^{38}$	$2.0 \cdot 10^{37}$	$1.2 \cdot 10^{28}$	$1.9 \cdot 10^{28}$	$9.3 \cdot 10^{27}$	–	–	$3.1 \cdot 10^{29}$
M101	$1.0 \cdot 10^{21}$	$4.3 \cdot 10^{38}$	$4.3 \cdot 10^{37}$	$1.4 \cdot 10^{28}$	$9.8 \cdot 10^{27}$	$1.5 \cdot 10^{28}$	–	–	$2.8 \cdot 10^{29}$
NGC2403	$2.9 \cdot 10^{21}$	$3.6 \cdot 10^{37}$	$1.1 \cdot 10^{36}$	$7.4 \cdot 10^{27}$	$5.4 \cdot 10^{27}$	$7.8 \cdot 10^{27}$	–	–	$1.4 \cdot 10^{28}$
NGC3077	$8.5 \cdot 10^{20}$	$3.2 \cdot 10^{37}$	$3.5 \cdot 10^{36}$	$1.4 \cdot 10^{28}$	–	–	–	–	$3.3 \cdot 10^{29}$
NGC3184	$2.7 \cdot 10^{20}$	$6.5 \cdot 10^{38}$	$4.3 \cdot 10^{36}$	$2.4 \cdot 10^{28}$	$1.4 \cdot 10^{28}$	$2.9 \cdot 10^{28}$	–	–	$3.6 \cdot 10^{29}$
NGC4214	$7.2 \cdot 10^{20}$	$2.7 \cdot 10^{37}$	0	$4.2 \cdot 10^{28}$	–	–	–	–	$7.3 \cdot 10^{29}$
NGC4449	$3.0 \cdot 10^{21}$	$2.2 \cdot 10^{38}$	$9.5 \cdot 10^{36}$	$6.8 \cdot 10^{28}$	–	–	–	–	$3.4 \cdot 10^{28}$

Note. Columns are as follows. (1) Average level of intrinsic N_H (2) Total unresolved luminosity in the 0.3 – 0.7 keV band. (3) Total luminosity of resolved supersoft sources in the 0.3 – 0.7 keV band. (4), (5), (6), (7), and (8) Observed L_X/L_K ratios in the 0.3 – 0.7 keV energy range for the entire galaxy, for its bulge, for its spiral arm regions, and for its interarm regions, respectively. The statistical errors vary between less than 1% and 5% (9) Predicted L_X/L_K ratios of supersoft sources in the single-degenerate scenario computed as described in the text; it is to be compared with column (4).

4.3 Unresolved X-ray binaries

The total (including resolved sources) X-ray emission of majority of galaxies is dominated by bright X-ray binaries. Their typical luminosity is in the range of $\sim 10^{35} - 10^{39} \text{ erg s}^{-1}$, therefore X-ray binaries fainter than the detection threshold inevitably contribute to the luminosity of the unresolved emission.

We estimate the contribution of LMXBs based on their luminosity function (Gilfanov 2004), assuming that their average spectrum is described by a power-law model with a slope of $\Gamma = 1.56$ (Irwin et al. 2003), and using a column density of 10^{21} cm^{-2} . Although the choice of N_H is somewhat arbitrary, its particular value within the observed limits does not affect our conclusion. With these conditions the contribution of unresolved LMXBs to the observed L_X/L_K ratios is in the range of $(6 \cdot 10^{24} - 1.1 \cdot 10^{26}) \text{ erg s}^{-1} L_{K,\odot}^{-1}$ in the 0.3 – 0.7 keV band, the upper limit is obviously associated with the worse source detection sensitivity.

As active star formation is associated with disk of spirals and irregular galaxies, we also estimate the contribution of unresolved HMXBs to the L_X/L_K ratios. We apply the luminosity function of Grimm et al. (2003) and the normalization according to Shtykovskiy & Gilfanov (2005) and assume an average power-law spectrum with slope of $\Gamma = 2$ with a column density of $N_H = 10^{21} \text{ cm}^{-2}$. Because the luminosity of HMXBs depends on the star-formation rate, their contribution to the L_X/L_K ratio will be highest in those galaxies where the star-formation rate per unit K-band luminosity (SFR/L_K) is highest assuming the same point source detection sensitivity. However, this latter parameter varies in our sample, therefore we estimated the unresolved fraction of HMXB luminosity for each galaxy individually. The highest values were obtained for irregular galaxies, in these the unresolved HMXBs contribute with $L_X/L_K = (4.1 - 7.6) \cdot 10^{26} \text{ erg s}^{-1} L_{K,\odot}^{-1}$, whereas in spirals we obtained $L_X/L_K = (4.1 \cdot 10^{25} - 5.8 \cdot 10^{26}) \text{ erg s}^{-1} L_{K,\odot}^{-1}$.

As we show in Sect. 5.1 the observed L_X/L_K ratios exceed the estimated contribution of LMXBs and HMXBs by at least $\sim 1 - 2$

orders of magnitude. Thus, we can exclude with high confidence that the population of unresolved X-ray binaries make a major contribution to the derived L_X/L_K ratios.

4.4 Faint unresolved sources

Those nuclear burning white dwarfs which have low color temperatures ($kT \lesssim 50 \text{ eV}$) and/or are significantly absorbed will not be detected by *Chandra* detectors as supersoft X-ray sources but will contribute to the unresolved emission. Besides these sources, however, there is a number of other types of X-ray sources, fainter than $\lesssim 10^{35} \text{ erg s}^{-1}$, contributing to the unresolved emission. These include coronally active binaries, cataclysmic variables, protostars, young stars, supernova remnants etc. The populations of different classes of sources were studied in the Solar neighborhood by Sazonov et al. (2006) based on *ROSAT* data. We used their specific luminosity value for the 0.1 – 2.4 keV range and estimated the 0.3 – 0.7 keV emissivity for these sources $L_X/L_K \sim \text{few} \times 10^{27} \text{ erg s}^{-1} L_{K,\odot}^{-1}$. This can make a sizable contribution to the unresolved emission in few galaxies with the lowest observed L_X/L_K ratios, but this contribution is not dominant.

5 RESULTS

The X-ray luminosities of the unresolved emission ($L_{X,unres}$) and resolved supersoft sources ($L_{X,SSS}$) are presented in the first columns of Table 2. With the exception of M81, resolved supersoft sources contribute less than about $\sim 1 - 10\%$ to the total luminosity in the 0.3 – 0.7 keV band. For M81, the two luminosities are nearly equal. Its case will be further discussed below, but we also note here that the luminosity of resolved supersoft sources in this galaxy is dominated by one very bright source with 0.3 – 0.7 keV luminosity of $1.2 \cdot 10^{38} \text{ erg s}^{-1}$.

5.1 L_X/L_K ratios

Further columns of Table 2 present L_X/L_K ratios for galaxies and their different structural components. The average L_X/L_K ratios range from $(5.4 \cdot 10^{27} - 6.8 \cdot 10^{28}) \text{ erg s}^{-1} L_{K,\odot}^{-1}$. Its lowest value is observed in M81. Due to its large angular extent, the disk of this galaxy was mostly outside the Chandra field of view. This may explain, at least in part, the smaller value of the L_X/L_K ratio. The other end of the range is represented by the irregular galaxy NGC4449.

Despite larger intrinsic absorption, the L_X/L_K ratios exceed by factor of about 2 – 20 those of early-type galaxies (Bogdán & Gilfanov 2010). This is further illustrated by Fig. 2 where X-ray luminosities are plotted against K-band luminosities. The early-type galaxy sample is taken from Bogdán & Gilfanov (2010). Although the contribution of bright resolved supersoft sources is included, it does not exceed $\sim 10\%$ (Table 2). Therefore this plot shows, essentially, the luminosity of unresolved emission. As in the case of early-type galaxies the contribution of unresolved X-ray binaries may be of some importance, we used X-ray luminosities transformed to the uniform source detection sensitivity of $2 \cdot 10^{36} \text{ erg s}^{-1}$. The straight lines show the emissivity of faint compact sources in the Solar neighborhood from Sazonov et al. (2006), including (solid) and excluding (dashed) the contribution of young stars. To convert their L_X/L_K ratio from the 0.1 – 2.4 keV to the 0.3 – 0.7 keV band we assumed $N_H = 10^{21} \text{ cm}^{-2}$ and an optically-thin thermal plasma emission model (MEKAL) with $kT = 0.3 \text{ keV}$; if a $\Gamma = 2$ power-law is assumed, the lines move downwards by a factor of ~ 2 . The agreement of soft X-ray luminosity of gas-poor early type galaxies with the old population of the Solar neighborhood is remarkable (we note that due to small investigated volume, the latter does not include any supersoft sources, however, as mentioned above, their contribution in the soft luminosity of early-type galaxies does not exceed $\sim 10 - 20\%$). Late-type galaxies, on the other hand, lie, with a large scatter, significantly above the line, corresponding to the Solar neighborhood. This is explained by contribution of the hot ionized ISM.

To further investigate spiral galaxies we measured L_X/L_K ratios for their bulges and disks. The separation was made based on near-infrared images. We did not find very large difference – the L_X/L_K ratios typically do not differ by more than a factor of ~ 2 , except for M74 where the disk value is larger by a factor of ~ 4 . There is a number of factors which may affect L_X/L_K ratios: the younger stellar population of the disk will tend to have higher L_X/L_K , whereas the more centrally concentrated hot X-ray emitting gas and the lower intrinsic absorption will increase its value in the bulge. Combination of these – and possibly other – effects may be responsible for observed scatter in L_X/L_K values.

Four galaxies in our sample (M51, M74, M81, and M83) have grand design spiral arms allowing us to measure L_X/L_K ratios of spiral arms and interarm regions separately, obtained values are given in Table 2. The arm and interarm regions were separated based on optical and near-infrared images. To our surprise, we did not find large difference between spirals arms and interarm regions, their L_X/L_K ratios being different by no more than $\sim 30\%$. The fact that the L_X/L_K ratios in spiral arms are not suppressed by the significantly higher intrinsic absorption may suggest that supersoft sources do not contribute significantly to the soft X-ray emission from the disks of spiral galaxies, but X-ray sources with harder spectrum dominate. The most likely candidate for such sources is the emission from ISM (Fig. 1).

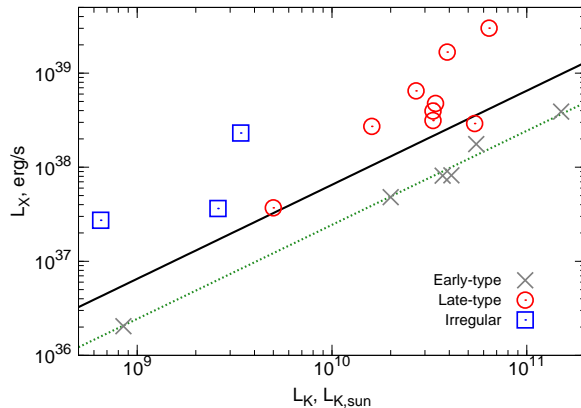


Figure 2. The 0.3 – 0.7 keV luminosity of unresolved emission and supersoft sources as a function of the K-band luminosity for early-type (Bogdán & Gilfanov 2010), spiral, and irregular galaxies. The solid line shows total emissivity of faint sources in the Solar neighborhood from Sazonov et al. (2006) recalculated to the 0.3 – 0.7 keV band as described in the text. The dashed line is the same but excluding contribution of young stars. The Sagittarius galaxy from Bogdán & Gilfanov (2010) falls outside the plot limits due to its small K-band luminosity but lies on the extrapolation of the dashed curve, following the trend of early-type galaxies.

5.2 Specific frequencies of supersoft sources

We also compared the numbers of resolved supersoft sources detected in bulges and disks and in spiral arms and in interarm regions. Due to their small number in each particular galaxy, we combined data for all nine spiral galaxies. Counting only sources with $L_X \geq 10^{36} \text{ erg s}^{-1}$ we found that 16 of them are located in bulges and 51 in disks. Taking into account the combined K-band luminosity of bulges ($1.1 \cdot 10^{11} L_{K,\odot}$) and disks ($2.0 \cdot 10^{11} L_{K,\odot}$) we derived the specific frequency of the supersoft sources of ≈ 1.4 in bulges and ≈ 2.6 per $10^{10} L_{K,\odot}$ in disks of spiral galaxies. As expected, but probably never confirmed quantitatively before, the specific frequency of supersoft sources in disks exceeds by factor of about 2 that of bulges.

For four grand design spiral galaxies we performed a similar investigation comparing spiral arms and interarm regions. There were 12 sources in spiral arms and 7 in interarm regions, whose K-band luminosities were $3.9 \cdot 10^{10} L_{K,\odot}$ and $1.8 \cdot 10^{10} L_{K,\odot}$ respectively. The specific frequencies of supersoft sources are close to each other: ≈ 3.1 and ≈ 3.9 per $10^{10} L_{K,\odot}$, respectively.

As a caveat we note that in calculating statistics of resolved supersoft sources we combined the data for different galaxies having different sensitivity limits (Table 1). In order to reduce this effect we counted only sources with $L_X \geq 10^{36} \text{ erg s}^{-1}$, however we made no attempt to perform an accurate incompleteness correction. This may affect somewhat the particular specific frequency values but would not change results of the comparison of different structural components of galaxies.

6 ROLE OF SUPERSOFT SOURCES AS PROGENITORS OF TYPE IA SUPERNOVAE

The observed L_X/L_K ratios allow us to constrain the role of supersoft sources as progenitors of SNe Ia. Although unlike the case of early-type galaxies, in late-type galaxies these constraints do not translate into global upper limits on the single degenerate scenario,

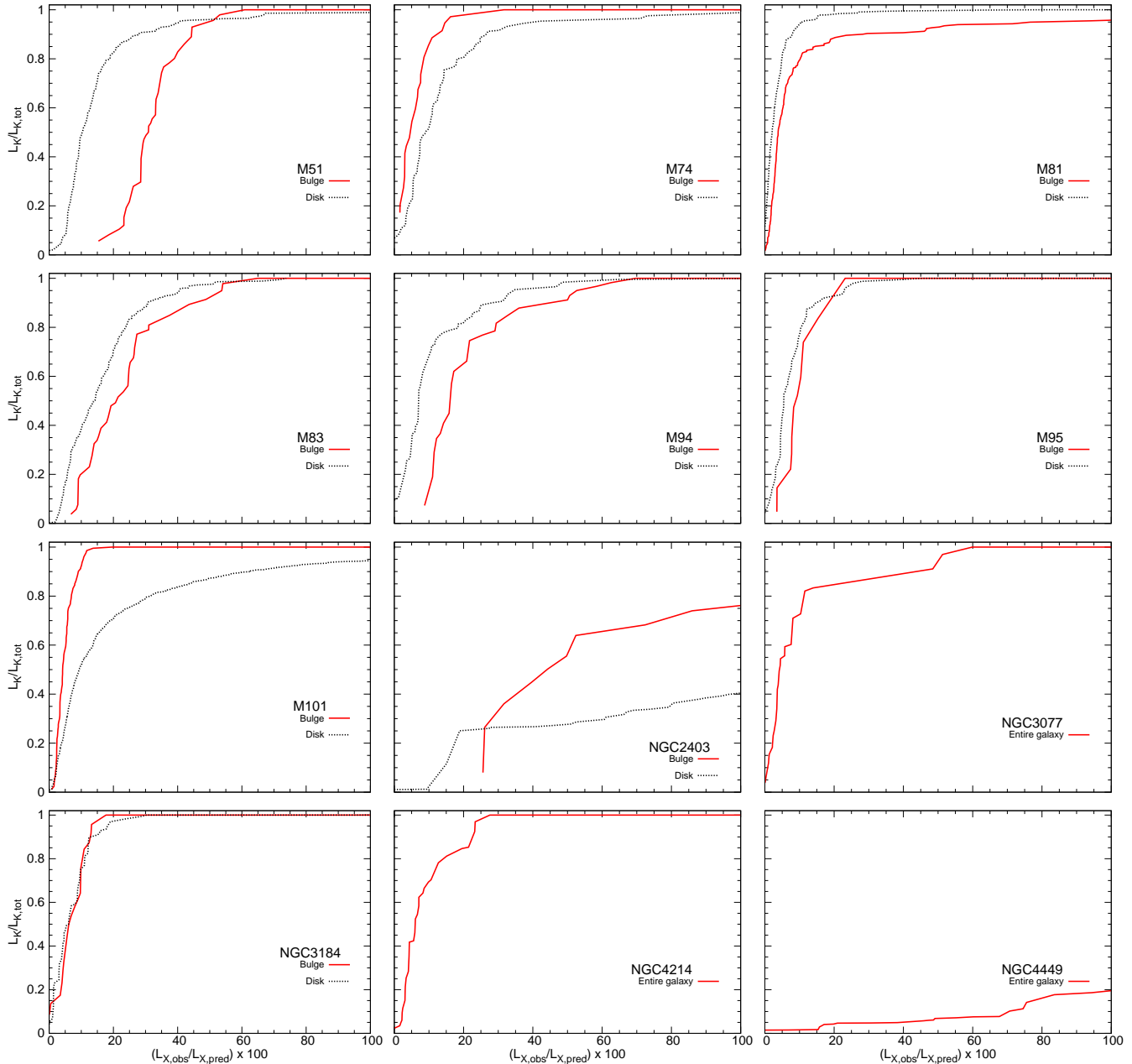


Figure 3. The fraction of K-band luminosity of the galaxy contained in the cells, in which the ratio of observed to predicted X-ray luminosities is smaller than a given value. The meaning of this plot is that it shows the fraction of the stellar mass of the galaxy where the contribution of the supersoft sources to the type Ia supernova rate, expressed in per cent, is smaller than the value shown on the x-axis.

they are important for understanding relative roles of different evolutionary channels. We therefore compare observed L_X/L_K ratios with the ones predicted in the single degenerate scenario.

In computing the predicted values we assumed that entire process of the mass accumulation by the white dwarfs proceeds in the regime with the nominal X-ray radiation efficiency, i.e. that the accreted material has solar composition and the photospheric radius of the nuclear burning hydrogen shell is close to the white dwarf radius. Particular calculations were conducted using approach and parameters of Gilfanov & Bogdán (2010), namely the initial white dwarf mass of $1.2 M_\odot$ and an accretion rate of $10^{-7} M_\odot/\text{yr}$. The SN Ia rate was assumed to be proportional to the K-band luminosity with the scale according to Mannucci et al.

(2005): $\dot{N}_{\text{SNIa}}/L_K = 3.5 \cdot 10^{-4} \text{ yr}^{-1}$ per $10^{10} L_{K,\odot}$ and $\dot{N}_{\text{SNIa}}/L_K = 8.8 \cdot 10^{-4} \text{ yr}^{-1}$ per $10^{10} L_{K,\odot}$ for the bulges and the disks of spiral galaxies and $\dot{N}_{\text{SNIa}}/L_K = 3.3 \cdot 10^{-3} \text{ yr}^{-1}$ per $10^{10} L_{K,\odot}$ for irregular galaxies.

6.1 Galaxy-averaged values

In comparing predicted luminosities with observations it is important to take into account strong and spatially varying absorption commonly present in late-type galaxies. In order to accomplish this we divided galaxies in sufficiently small cells. In choosing the cell size we required that each contained at least 30 X-ray counts in the 0.3 – 0.7 keV band, necessary for the spatially resolved analysis

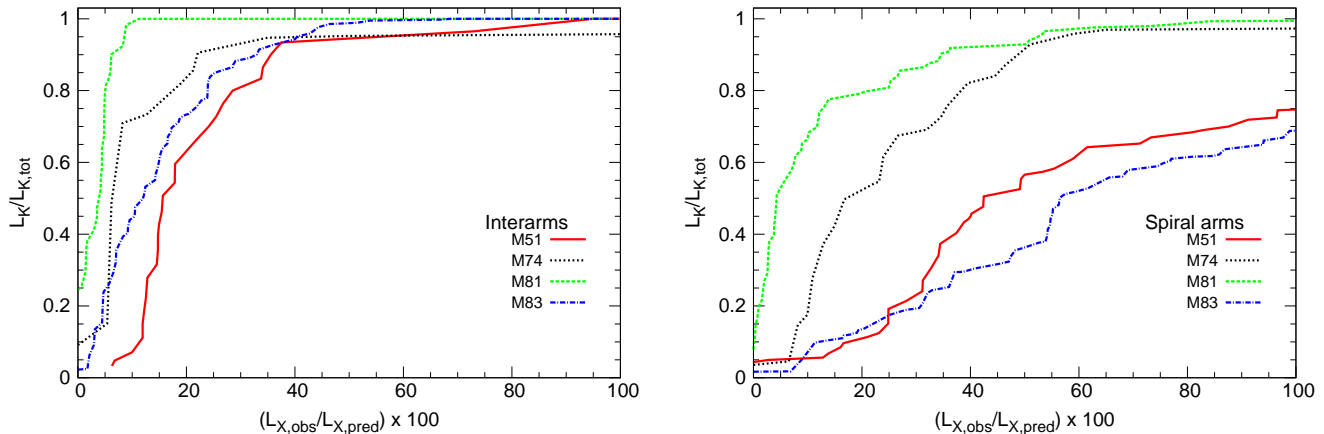


Figure 4. Same as Fig. 3 but for interarm regions (left panel) and spiral arm regions (right) for the four grand design spiral arm galaxies in our sample.

described below. Thus, the number of cells per galaxy depends on their surface brightness and Chandra exposure time and varied from 28 in case of NGC3077 to 1065 for M101. The typical K-band luminosity within one cell was in the $10^7 - 10^8 L_{K,\odot}$ range and size was between $\sim 5 - 30''$.

In each cell the supernova rate was computed from its K-band luminosity and the X-ray luminosity of nuclear burning white dwarfs was computed and absorption (intrinsic, determined for each cell from HI maps, and Galactic) was applied. The luminosities of all cells in a galaxy were summed and divided by its K-band luminosity to give the average predicted L_X/L_K ratio. The so computed values are presented in the last column of Table 2. By the method of calculation they present galactic average and are to be compared with observed values listed in the column (4), marked $(L_X/L_K)_{total}$.

Table 2 shows that for majority of galaxies predicted L_X/L_K ratios exceed observed values by a factor of $\sim 7 - 30$. For these galaxies we can place upper limits of $\sim 3 - 15\%$ on the contribution of supersoft sources to the SN Ia rate. For few galaxies, M94, NGC 2403 and NGC3077, the difference is ~ 2 times. In the case of NGC4449 predicted X-ray luminosity is ~ 2 times smaller than the observed value. For these galaxies no meaningful upper limits can be placed. We note that the latter galaxy has largest N_H and L_X/L_K ratio. It is further discussed in the Sect. 6.4.

6.2 Spatially resolved analysis

Using the results of this calculation it is also possible to compare prediction of the model with observation in a more detailed, spatially resolved manner, computing the ratio of the observed luminosity to the predicted value in each individual cell. To present results of this analysis we plot in the Fig. 3 the fraction of K-band luminosity of the galaxy contained in the cells, in which the ratio of observed to predicted X-ray luminosity is smaller than a given value. The meaning of this plot is that it shows the fraction of the stellar mass of the galaxy where the contribution of the supersoft sources to the type Ia supernova rate is smaller than the given value.

The plot reveals a large variations between galaxies in our sample. In several of them, M74, M81, M95 and NGC3184, supersoft sources cannot contribute more than $\sim 5 - 10\%$ to the type Ia supernova rate in more than $\sim 80 - 90\%$ of their mass. The other end of the range is represented by NGC2403 and NGC4449, in which supersoft sources could, in principle, be progenitors of

a large fraction of type Ia supernovae without contradicting X-ray observations.

6.3 Spiral arms and interarm regions

We applied similar approach to analyze spiral arms and interarm regions in the four grand design spiral galaxies. In computing the SN Ia rates we note that scale factors from Mannucci et al. (2005) refer to entire galaxies, therefore it may be inaccurate to use them in the analysis of arm and interarm regions. Instead, we use results of Sullivan et al. (2006) who decomposed the SN Ia rate into a mass related and a star-formation related components. Namely, we assumed scale factors of $5.3 \cdot 10^{-14} \text{ SNe yr}^{-1} M_\odot^{-1}$ and $3.9 \cdot 10^{-4} \text{ SNe yr}^{-1} (M_\odot \text{ yr}^{-1})$. The stellar mass in cells was determined from their K-band luminosity assuming a mass-to-light ratio of $M_\star/L_K = 0.8$. The star-formation rate was computed based on *Spitzer* far-infrared images as described in Sect. 3.2. The resulting upper limits are plotted in Fig. 4 using the same approach as in Fig. 3. The plot shows that upper limits for interarm regions are generally tighter than for the disks as a whole. Overall, in more than $\sim 80\%$ of mass the contribution of supersoft sources to the SN Ia rate is less than $\sim 5 - 30\%$. In the spiral arms, on the contrary, no constraining upper limits can be obtained in three out of four galaxies – the supersoft sources can, in principle, be progenitors of a large fraction of SN Ia.

A number of studies (e.g. Scannapieco & Bildsten 2005; Mannucci et al. 2006) indicate that SNe Ia originate from two sub-populations, often designated as prompt and delayed populations. The prompt population is believed to dominate at ages $\lesssim 10^8$ years, therefore this component is presumably associated with star-forming regions of galaxies, whereas the delayed population is producing SNe Ia in older stellar populations. According to the results of our spatially resolved analysis we find that a model, in which the major fraction of the prompt population originates from supersoft sources, does not contradict our X-ray data.

6.4 Dependence of upper limits on absorption and star-formation rate

The obtained upper limits vary significantly between galaxies, from a few per cent level to unconstraining values of tens of per cent. One may ask a question, whether these variations are a

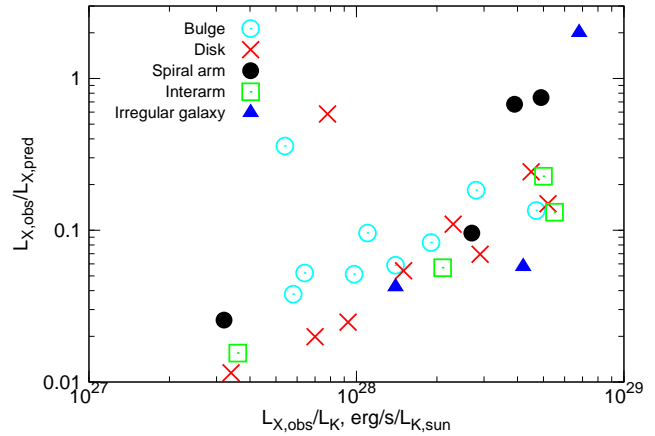
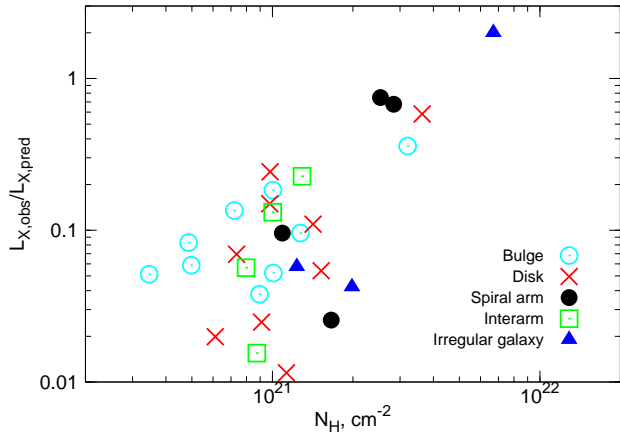


Figure 5. Ratio of observed luminosity in the 0.3 – 0.7 keV band to the luminosity of supersoft sources predicted in the single degenerate scenario, for entire galaxies and their structural components, versus average N_H and L_X/L_K ratio.

result of different levels of contamination and absorption in different galaxies or do indeed reflect varying contribution of supersoft sources. In an attempt to answer this question we plot in Fig. 5 the ratio of the observed X-ray luminosity to the luminosity of supersoft sources predicted in the single degenerate scenario, L_X^{obs}/L_X^{pred} , versus the N_H value and L_X/L_K ratio. The predicted luminosity was computed by the method described earlier in this section. The plots show clear correlations – the observed-to-predicted luminosity ratio increases with the column density and with specific luminosity of unresolved X-ray emission. This may indicate that variations in the upper limits are caused by variations in absorption and in the level of contamination.

On the other hand, in a picture, which is not entirely implausible, the role of supersoft sources as SN Ia progenitors may increase in star-forming galaxies. Therefore one may expect a positive correlation of the luminosity of supersoft sources with the star-formation rate. To investigate this, we plot in Fig. 6 the observed-to-predicted luminosity ratio versus specific star-formation rate. The plot does show some evidence of such a correlation, in an apparent contradiction to the tentative conclusion made above. It should be taken into account however, that star-forming galaxies tend to have larger N_H and brighter levels of the diffuse emission, which may produce secondary correlations.

7 CONCLUSIONS

The aim of this study was to measure soft band L_X/L_K ratios in late-type galaxies. Although these ratios are of interest on their own, our primary goal was to derive constraints on X-ray emission from nuclear burning white dwarfs and to constrain the role of supersoft sources as progenitors of SNe Ia. To this end we used an extensive set of archival *Chandra* observations of a sample of twelve late-type galaxies, which included nine spiral and three irregular galaxies. In selecting our sample we demanded a source detection sensitivity of at least $5 \cdot 10^{36}$ erg s $^{-1}$ allowing the removal of bright X-ray binaries. We also required the existence of publicly available HI maps in order to measure the intrinsic absorption.

The observed 0.3–0.7 keV band L_X/L_K ratios range from $5.4 \cdot 10^{27}$ to $6.8 \cdot 10^{28}$ erg s $^{-1}$ $L_{K,\odot}^{-1}$, significantly exceeding those in early-type galaxies. Based on the spectral analysis we tentatively suggest that the primary reason for this difference is the soft X-ray emission

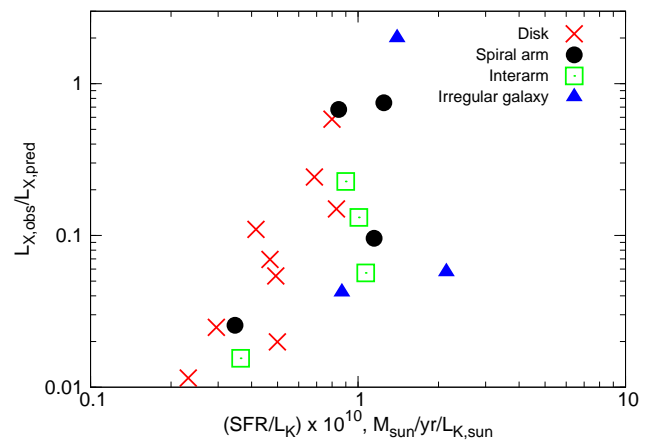


Figure 6. Ratio of observed luminosity in the 0.3–0.7 keV band to the luminosity of supersoft sources predicted in the single degenerate scenario, for entire galaxies and their structural components, versus star-formation rate.

from hot ionized ISM with the temperature of $kT \sim 0.2 - 0.4$ keV. X-ray emission from young stars in star-forming regions may also contribute. On a more detailed level we determine L_X/L_K ratios for bulges and disks of spiral galaxies separately and for majority of them found a factor of $\sim 2 - 4$ difference. Surprisingly, the sign of this difference was different in different galaxies, indicating the complexity of distribution of various X-ray emitting components in spiral galaxies. Furthermore, in four grand design spiral galaxies we separated spiral arms and interarm regions and found that their L_X/L_K ratios do not differ by more than $\sim 30\%$.

We investigated the role of supersoft sources as progenitors of SNe Ia. As a measure of their contribution we calculated the ratio of the observed soft X-ray luminosity to the luminosity predicted by the single degenerate scenario. The latter was computed assuming the nominal X-ray radiation efficiency of nuclear burning white dwarfs, as expected in the standard picture of supersoft sources (Kahabka & van den Heuvel 1997). We find that for majority of galaxies the predicted luminosity exceeds observed values by a factor of $\sim 7 - 30$. Taken at the face value, these numbers imply upper limit of $\sim 3 - 15\%$ on the contribution of supersoft sources to the SN Ia rate. For a few galaxies observed and predicted luminosities

ties are comparable, therefore no constraining upper limits can be placed, including NGC4449, where predicted luminosity is smaller than the observed one. The spatially resolved analysis yielded similar results. Correlations of the upper limits with N_{H} and $L_{\text{X}}/L_{\text{K}}$ ratios suggest that large scatter in upper limit may be a result of different level of contamination and absorption in different galaxies.

It is important to realize that for the late-type galaxies, upper limits on the contribution of supersoft sources to SN Ia rate do not translate into upper limits on the single degenerate scenario in general. In young stellar environment several possibilities may exist, that X-ray emission from nuclear burning white dwarfs is significantly suppressed (e.g. Hachisu et al. 1996; Iben & Tutukov 1994). Note that these possibilities are not expected to play significant role in early-type galaxies considered in Gilfanov & Bogdán (2010), due to the old age of their stellar populations.

Finally, we investigated the specific frequency of bright supersoft sources in bulges and disks of spiral galaxies and found significant difference, the supersoft sources being factor of ~ 2 times more frequent (per unit K-band luminosity) in the disks than in the bulges.

Acknowledgements. We thank the anonymous referee for his/her useful comments. Á. Bogdán is grateful to Stefano Mineo for helpful discussions about measurements of star formation rates. This research has made use of *Chandra* archival data provided by the *Chandra* X-ray Center. The publication makes use of software provided by the *Chandra* X-ray Center (CXC) in the application package CIAO. The *Spitzer Space Telescope* is operated by the Jet Propulsion Laboratory, California Institute of Technology, under contract with the National Aeronautics and Space Administration. This publication makes use of data products from the Two Micron All Sky Survey, which is a joint project of the University of Massachusetts and the Infrared Processing and Analysis Center/California Institute of Technology, funded by the National Aeronautics and Space Administration and the National Science Foundation. This work makes use of THINGS, “The HI Nearby Galaxy Survey”.

REFERENCES

- Bavouzet, N., Dole, H., Le Floch, E., Caputi, K. I., Lagache, G., Kochanek, C. S., 2008, *A&A*, 479, 83
- Bell, E. F., 2003, *ApJ*, 586, 794
- Bogdán, Á. & Gilfanov, M., 2008, *MNRAS*, 388, 56
- Bogdán, Á. & Gilfanov, M., 2010, *A&A*, 512, 16
- Dickey, J. M., Lockman, F. J., 1990, *ARA&A*, 28, 215
- Di Stefano, R. & Kong, A. K. H., 2003, *ApJ*, 592, 884
- Di Stefano, R., 2010, *ApJ*, 712, 728
- Freedman, W. L., et al., 2001, *ApJ*, 553, 47
- Gilfanov, M., 2004, *MNRAS*, 349, 146
- Gilfanov, M. & Bogdán, Á., 2010, *Nature*, 463, 924
- Grimm, H.-J., Gilfanov, M. & Sunyaev, R., *MNRAS*, 339, 793
- Hachisu, I., Kato, M. & Nomoto, K., 1996, *ApJ*, 470, 97
- Hachisu, I., Kato, M. & Nomoto, K., 1999, *ApJ*, 522, 487
- Iben, I. Jr. & Tutukov, A. V. 1994, *ApJ*, 431, 264
- Irwin, J. A., Athney, A. E. & Bregman, J. N. 2003, *ApJ*, 587, 356
- Jarrett, T. H., Chester, T., Cutri, R., et al., 2003, *AJ*, 125, 525
- Kahabka, P. & van den Heuvel, E. P. J., 1997, *ARA&A*, 35, 69
- Karachentsev, I. D., Karachentseva, V. E., Huchtmeier, W. K. & Makarov, D. I., 2004, *AJ*, 127, 2031
- Leonard, D. C., et al., 2002, *AJ*, 124, 2490
- Mannucci, F., Della Valle, M., Panagia, N., Cappellaro, E., Cresci, G., Maiolino, R., Petrosian, A. & Turatto, M., 2005, *A&A*, 433, 807
- Mannucci, F., Della Valle, M. & Panagia, N., 2006, *MNRAS*, 370, 773
- Nomoto, K., Saio, H., Kato, M. & Hachisu, I., 2007, *ApJ*, 663, 1269
- Perlmutter, S., Aldering, G., Goldhaber, G., et al., 1999, *ApJ*, 517, 565
- Riess, A. G., Filippenko, A. V., Challis, P., et al., 1998, *AJ*, 116, 1009
- Sazonov, S., Revnivtsev, M., Gilfanov, M., Churazov, E. & Sunyaev, R., 2006, *A&A*, 450, 117
- Scannapieco, E. & Bildsten, L., 2005, *ApJ*, 629, 85
- Shtykovskiy, P. & Gilfanov, M., 2005, *MNRAS*, 362, 879
- Sullivan, M., et al., 2006, *ApJ*, 648, 868
- Walter, F., Brinks, E., de Blok, W. J. G., Bigiel, F., Kennicutt, R. C., Thornley, M. D. & Leroy, A., 2008, *AJ*, 136, 2563